CHAPTER 2

REVIEW OF LITERATURE

This chapter contains a critical review of the existing literature on the various techniques for synthesising graphene and its role in improving the friction and wear performance of the bodies in relative motion. The chapter begins with highlighting the importance of surface interactions in governing the wear behaviour of mating bodies, which is followed by a brief introduction to phenomena of friction and wear. A brief description of the different theories of friction and types of wear along with the methods of minimising them also forms a part of the chapter. Further, an exhaustive literature regarding the graphene, a 2D solid lubricant, including its structure, properties, applications, methods of synthesis has been presented. Special attention has been given to the researches being conducted in regard to the application of graphene both as a coating and as an additive in lubricant, in improving the friction and wear characteristics of a tribo-pair. At the end, the formulation of the problem for the current investigation has been included.

2.1 SURFACE INTERACTIONS AND WEAR

Whenever two surfaces come into contact with each other, the forces of action and reaction come into play, and the surfaces are said to undergo surface interaction. Surface interaction is an important phenomenon in various engineering situations, including tribological aspects and it is affected by a number of factors such as surface roughness, contact area, surface material etc.

All engineering surfaces are rough. This is their first important characteristics, which is tribologically significant. The other properties which govern the surface interaction behaviour are the volume properties which relate to the contacting bodies as a whole and the surface properties which determine the nature of contacting interface between these bodies. **Surface roughness** plays a significant role in determining how a surface will interact with others. Surface roughness is quantified by the deviations in the direction of the normal vector of a real surface from its ideal form. If these deviations are large, the surface is considered as rough; if they are small, the surface is considered as smooth. The smooth surfaces usually have a lower value of friction coefficient and undergo wear comparatively slower than rough surfaces. Surface roughness is usually characterised by R_a (arithmetic average) and R_q (root mean square). S_k (skewness), K (kurtosis), R_t (maximum peak-to-valley height), R_z (average peak-to-valley height), R_{pm} (average peak-to-mean height), R_p (maximum peak height), and R_v (maximum valley depth) are other amplitude parameters to measure the surface roughness. Surface roughness can be measured by using various instruments such as surface roughness tester, atomic force microscope, profilometer, scanning laser microscope (Bhushan, 1999).

2.1.1 SURFACE CONTACTS

When two nominally flat surfaces are brought in contact by applying a normal load, they touch each other at the tips of asperities only. Hence the real area of contact is much less compared to the apparent area of contact (Archard, 1980). The small regions where the contacting surfaces are close together, are referred to as “junctions” and the sum of the areas of all the junctions constitute the real area of contact, A_r. The total interfacial area, consisting both of real area of contact, A_r, and those regions which appear

as if contact might have been made there (but was not) is taken as the apparent area of contact, A_a. The numbers, size and distance of separation of junctions play a dominant role in influencing the friction and wear behaviour of materials in sliding contact.

According to Rabinowicz (1965), when the deformation of the asperity is plastic in a single asperity contact, the real area of contact is directly proportional to normal load and is given by the equation,

$$A_r = \frac{L}{H} \tag{2.1}$$

Where, L is the average load and H is the initial hardness of the softer of the two materials in contact.

Holm (1958) and Bowden and Tabor (1954) have shown that the limiting value of the pressure at the contacting interface is set by the hardness of the softer of the two materials and the real area of contact is given by the above equation. Further, it has been concluded by them that the real area of contact is independent of the surface topography and the apparent area of contact.

2.1.2 FRICTION

Friction is defined as the resistance to motion encountered by one body when it moves or tries to move over the other body. Friction is a system response, not a material property. The friction force arises due to the relative movement of interacting asperities of mating surfaces. The friction force is the resistive tangential force, which always acts in the opposite direction of motion. Depending on applications, friction force may be either maximised (brakes, clutches, power transmission drive) or minimised (bearings).

The ratio of friction force to normal load is termed as the coefficient of friction and it is dependent upon the mating pair, surface cleanliness, and operating conditions such as sliding velocity, contact pressure, temperature, and environment, etc.

Amontons (1699) enunciated two fundamental laws of intrinsic friction, which are generally well followed over a wide range of applications. Another law, i.e., third law, was added by Coulomb (1785). The third law has exceptions and is not obeyed in general. It was observed that the friction coefficient decreases with an increase in sliding velocity, which may be due to thermal softening at the interface (Rabinowicz, 1965). Bowden and Tabor (1964) and Dowson (1978) reported the three basic laws of friction enunciated by Amontons (1699) and Coulomb (1785), which are given below:

i. The force of friction is directly proportional to the applied normal load.
ii. The force of friction is independent of the apparent area of contact between the contacting bodies.
iii. Kinetic friction is independent of the sliding velocity once the motion starts.

Bowden and Tabor (1950) proposed the adhesion theory of friction which states that, when relative motion is imparted to the interface by applying a tangential force, each pair of contacting asperities weld together and shear to accommodate the relative motion. The friction arises from two sources: an adhesion force developed at the real area of contact between the surfaces (asperity junctions) and a delamination force needed to plough the asperities of the harder surface through the softer ones.

According to this theory, major force of friction is the force required to shear the junctions formed between the two bodies at the real area of contact. This force of friction is given by:

$$F = \tau A_r \tag{2.2}$$

Where, τ is the shear strength of these junctions, which is a function of the materials of the bodies (and, of any intervening surface film). The coefficient of friction (μ) is then given by the following equation:

$$\mu = \frac{F}{L} = \frac{\tau\, A_r}{H\, A_r} = \frac{\tau}{H} \tag{2.3}$$

Thus friction coefficient can be taken as the ratio of two quantities τ and H, representing respectively, the resistance to plastic flow of the weaker of the contacting materials in shear and compression. The above theory has been criticised by various researchers as it assumes only a simple model of asperity deformation.

Suh and Sin (1981) have established that there are three basic mechanisms responsible for the origin of friction. These are (i) asperity deformation, (ii) ploughing and (iii) adhesion. The asperity deformation determines the static coefficient of friction and also, affects the dynamic coefficient of friction. Since new asperities are generated only with the formation of delaminated wear particles, which requires a large number of cyclic loading by the asperities of the counterface, the contribution of the asperity deformation to the dynamic Friction coefficient is not large relative to those by ploughing and adhesion. The ploughing component of the frictional force can be due to the penetration of hard asperities or due to penetration of wear particles into the softer material. When both the mating surface are of equal hardness, the particle can penetrate both the surfaces. If one of the surfaces is very hard and smooth, the wear particle will simply slide along the hard surface, and no ploughing would occur. However, when the

hard surface is very rough, wear particles may anchor in the hard surface and plough the soft surface (Sin et al., 1979).

Liu et al., (1992) have indicated that friction force arises due to the interaction between the asperities as (a) adhesion at the contacting points and (b) deformation either elastic or plastic of the asperities by the load. The force required to overcome friction will consist of the force required to shear the adhesion bond F_a and the force required to deform elastically or plastically, F_d the obstructing asperities of the relatively softer material in the path of the asperities of the relatively harder material. The coefficient of friction μ is, therefore, expressed as:

$$\mu = \frac{F_a + F_d}{L} = \mu_a + \mu_d \tag{2.4}$$

Where, L is the applied normal load on the contacting surface, μ_a and μ_d are the friction coefficients due to adhesion and deformation, respectively.

2.1.3 WEAR

Wear is defined as the surface damage or progressive loss of material from one or both mating surfaces in contact due to interfacial rubbing relative to each other. It occurs mainly through the interaction of surfaces at asperities. Like friction, wear is also a system response, not a material property. Depending on the applications, wear can be either desirable or not desirable. Controlled productive wear such as writing with a pencil, machining, polishing, and shaving, is desirable, while it is undesirable in most of the machine applications such as bearings, seals, gears, and cams (Bhushan, 1999).

2.1.3.1 Types of Wear

Wear can be categorised based on mechanisms and conditions, which prevail during material removal. It may be classified on the basis of the appearance of the worn parts or mechanisms and conditions, which prevail during material removal. The types of wear classified according to the wear mechanisms and conditions are: (i) adhesive wear (ii) abrasive wear (iii) erosive wear (iv) impact wear (v) fatigue wear (vi) corrosive wear.

Adhesive wear is associated with low sliding velocity, small load and smooth surfaces. This is a universal type of wear that can occur in every machine and hard to be eliminated but can only be reduced. Adhesion processes involve the interaction of asperities on two opposing surfaces in relative motion. When the asperities come in close contact, they may weld together, forming a bond at the junction, which has rupture strength greater than the yield strength of one of the contacting solids. In such a case fracture may take place in one of the asperities resulting in the transfer of material from one contacting body to other. **Abrasive wear** occurs when two surfaces, one of which is harder and rougher than the other, are in sliding contact. Abrasive wear is the removal or the displacement of material from one surface by the harder asperities of another surface or by harder, loose particles. This type of wear is dangerous because it can occur suddenly with the introduction of a contaminant and may lead to high wear rates and extensive damage to the surface. **Erosive wear** is a combined process of repeated deformation and cutting. When a solid surface is gradually worn away by the action of fluids and particles, it is called erosion. Erosion of materials can take place under four different conditions: (1) impingement of solid particles against a solid surface, (2) impingement of liquid droplets against a solid surface, (3) flow of hot gases over a solid surface and (4) cavitation at a solid surface in liquid media. The most important form of erosion is that

caused by solid particle impingement. **Impact wear** arises from the repetitive impact of two surfaces, which differs from the impact of solid particles on a surface causing erosive wear. **Fatigue wear** refers to the cyclically repeated imposition of a stress state on the surface of a component, inducing a small degree of mechanical damage in the surface and subsurface regions with each stress pulse. Ultimately, the damage accumulation leads to a failure by deformation and/or fracture at the surface. **Corrosive wear** is the synergistic effect of chemical reaction at a surface with any of the mechanical wear mechanisms. In a corrosive environment, sliding surfaces experience corrosive wear. However, in some cases, the reaction layer protects the surface or even act as a lubricant.

2.2 MINIMISATION OF FRICTION AND WEAR

Since wear causes wastage of material directly leading to loss of mechanical performance and involving the considerable cost involvement, it should be minimised as much as possible. Similarly, the friction between the surfaces involves enormous economic loss in terms of energy. Some of the major techniques employed to minimised friction and wear are Microstructural treatment, Lubrication, Materials substitution or use of composites and Surface modification (including surface texturing, and coating).

According to Bhushan (1999), microstructural treatment pertains to increase in the surface hardness of the material, which causes an improvement in wear resistance. It is a relatively cheap way to improve tribological properties and do not require any special material, unlike other ways to control friction and wear. A martensitic structure with a tough, ductile core may be produced by quenching after case hardening of thin surface shell of ferrous metal. Flame hardening, induction hardening, laser hardening,

electron beam hardening, work hardening, metalworking, shot peening are the most common treatments employed for treatment of microstructure.

Lubrication is an old and effective way to reduce friction as well as wear by imposing a substance named lubricant between the surfaces in relative motion. The lubricant may be solid, liquid or gas. The use of lubrication allows the smooth and continuous operation of machine/component, thus leading to reduced friction and wear. Friction and wear can be reduced effectively by material substitution or by use of composites. In this, a commercially used material is replaced by any other material or composite with superior anti-wear and anti-friction properties.

The surface treatment is the modification of a surface to reduce friction and wear, which is mostly in the form of surface texturing or coating. Surface texturing is the surface modification process in which different patterns of micro or nanoscale are created on the surface. The texture made on the surface can serve as a storage pocket for liquid lubricant (in full fluid-film and mixed lubrication) or wear debris (in dry and boundary lubrication), which help in significant improvement in the tribological performance. However, the selection of inappropriate texturing parameters may also lead to increased friction and wear. (Grützmacher et al., 2019; Vencl et al., 2019). On the other hand, coating (from the tribological point of view) is a layer deposited on the material of interest to enhance its tribological properties. Depending on the nature of the coated surface, the coating can be classified as hard (wear-resistant coatings) and soft (low-friction coatings).

2.3 LUBRICATION

Lubrication is the oldest and most popular technique to reduce both friction and wear. Lubricant is a substance that is used to facilitate the relative motion of solid bodies by imposing it between interacting surfaces, and the action of applying lubricant between the interacting surface to reduce the friction and wear is termed as lubrication. Lubricants also help to reduce the heat generated between the interfaces. Based on the physical state, the lubricants may be classified as:

i. **Liquid lubricants:** Mineral or synthetic oils, vegetable oils, animal oils
ii. **Semi-solid lubricants:** Greases
iii. **Solid lubricants:** Graphite, MoS_2, hBN
iv. **Gaseous lubricants:** Nitrogen, Helium

Liquid lubricants reduce friction and wear between two interacting surfaces by providing a continuous liquid layer in-between them. Good lubricating oil must possess the following properties: (a) low pressure (or high boiling point), (b) adequate viscosity for particular service conditions, (c) low freezing point, (d) high oxidation resistance. (e) heat stability, (f) non-corrosive properties, (g) stability to decomposition at the operating temperatures. Liquid lubricant may be classified on the basis of the type of base oil such as mineral oil, vegetable oil, animal oil, synthetic oil etc.,

Semi-solid lubricants are used in several applications such as anti-friction and roller bearing, where either the liquid lubricants cannot be conveniently applied, or a thick film is required. Greases are the most commonly used semi-solid lubricants which are usually produced by emulsifying the oil (mineral, synthetic or vegetable) with soap.

The distinguishing feature of a grease is its high viscosity. The consistency of produced grease is dependent on the amount of oil added. The structure of grease is similar to gel. Due to higher shear and frictional resistance, the grease can support a comparatively higher load than liquid lubricants.

Solid lubricants are applied mostly in the form of a coating or as additives in liquid lubricants, greases and composites. A solid lubricant is a material used as powder or thin-film, which reduces friction and wear of contacting surfaces in relative motion and provides protection from damage. Graphite and molybdenum disulfide are the two most commonly used solid lubricants.

Gaseous lubricants involve the establishment of the gas film between the lubricating surface which can provide the lubrication. Gas lubricants possess the lowest viscosity and mostly used in aerostatic and aerodynamic bearing. Air, nitrogen, and helium are the most common gaseous lubricants.

2.4 SOLID LUBRICANTS

Solid lubricants or dry lubricants are the lubricant in the solid phase and have the capability of reducing the friction as well as wear between the two interacting surfaces. Solid lubricants have several advantages over conventional lubricants, including superior cleanliness. Solid lubricants can work well under the extreme conditions of temperature and pressure. Lamellar solids, soft metals, diamond, and DLC films and lubricious oxides are examples of solid lubricants. Solid lubricants have the following advantages over conventional liquid lubricants:

i. Solid lubricants can provide lubrication under extreme conditions of temperature and pressure.
ii. Solid lubrication can avoid the contamination of dust or grit particles.
iii. Solid lubricants may be applied in inaccessible location, where it is hard to apply liquid lubricants or greases.
iv. Solid lubricants are best suited for intermittent loading conditions.
v. Solid lubricants may also be used as additive.

2.4.1 LAMELLAR SOLID LUBRICANTS

Lamellar solid lubricants are made of layers stacked over one another, and these layers are termed as lamellae. The mechanism behind low friction of lamellar solid lubricants involves the sliding of adjacent lamellas over one other at relatively low shear stresses, as shown in Fig. 2.1. The lamellar solids must possess three characteristics feature from lubrication point of view, which are:

i. The lamellar structure of solid must deforms at very low shear stress levels;
ii. The lamellar solid must adhere to the worn surface firmly;
iii. The lamellar solid should not decompose or chemically degrade at operating temperature and in the environment.

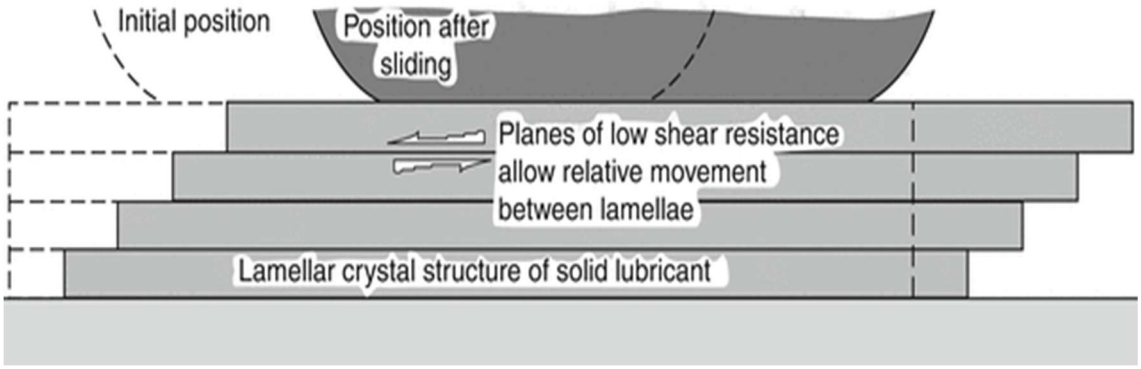

Fig. 2.1 Lubrication mechanism of lamellar solid lubricants. (Stachowiak and Batchelor, 2001)

Graphite, molybdenum disulphide and hexagonal boron nitride are the most traditional lamellar solid lubricants. The graphite consists of one atom thick hexagonal 2-dimensional sheets stacked over one another. The molybdenum disulfide has a sandwich-like structure consisting of a layer Mo atoms between two layers of S atoms. The hexagonal boron nitride consists of covalently bonded atoms of boron (B) and nitrogen (N), in a hexagonal plane with the angle 120° between two bonds. Each boron atom is bonded to three nitrogen atoms and vice versa.

Recently, graphene, which is one intercalation layer of graphite, has also attracted the attention of scientists/engineers working in the area of tribology due to its structure and properties. The extremely high mechanical strength, easy interlayer shearing, excellent young's modulus, low surface energy, good conductivity, and high thermal and chemical stability make it a potential candidate to be used as a solid lubricant. Several studies (Lee at al., 2010; Berman et al., 2013; Fan and wang, 2015; Yang et al., 2017; Hong et al., 2018; Mohan et al., 2018; Sun and Du, 2019) have reported the tribological potential of graphene as solid lubricating coating, as an additive in lubricant, and as a reinforcement to synthesise (metal/polymer/ceramic) based composites.

2.5 GRAPHENE

Graphene, the first 2D material and a crystalline allotrope of carbon, is a one-atom-thick layer of graphite. It is the mother of all graphitic forms, including graphite, carbon nanotube, and fullerenes, as shown in Fig. 2.2. It can be stacked into graphite, rolled into 1D nanotubes, or wrapped up into 0D fullerenes. Graphene consists of sp^2-hybridised carbon atoms arranged on a hexagonal lattice forming a honeycomb-like structure. Although, Graphene came into existence experimentally during the previous decades, but it has a lengthy theoretical background of more than 70 years. Graphene was introduced the first time theoretically as a single hexagonal layer of graphite by Wallace (1947). Geim and Novoselov isolated a single atomic layer of carbon for the first time in 2004 through repeated peeling of graphite using a scotch tape (Novoselov et al., 2004).

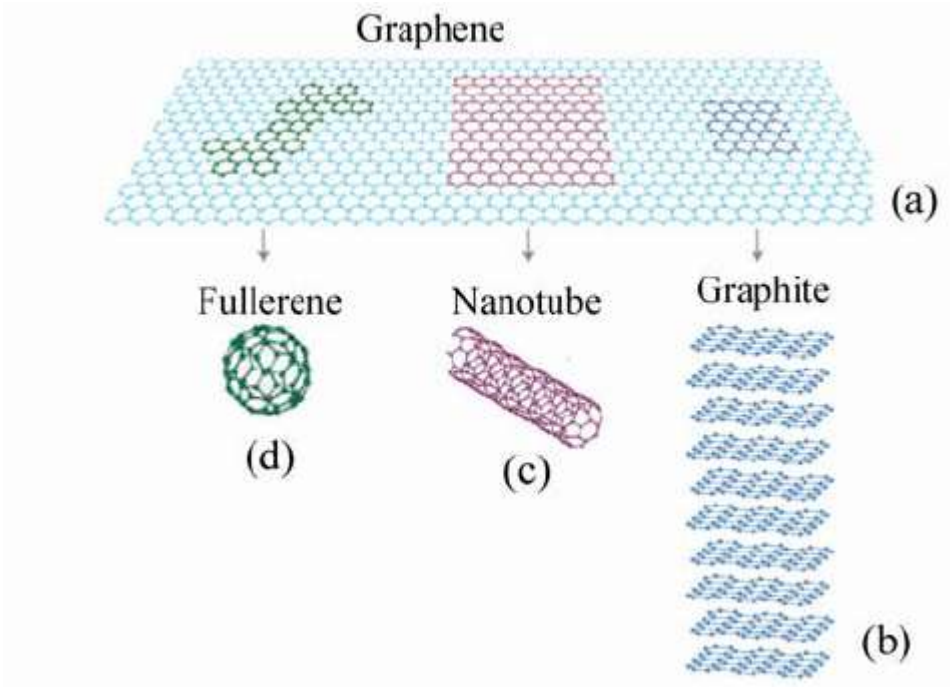

Fig. 2.2 Schematic structure of (a) graphene, (b) graphite, (c) carbon nanotube and (d) fullerene. (Giannazzo et al., 2011)

2.5.1 STRUCTURE, PROPERTIES AND APPLICATIONS

The graphene, a crystalline allotrope of carbon, consists of carbon atoms densely packed in a hexagonal pattern, which can be said to resemble a chicken wire. The distance between the two carbon atoms is about 1.42 Å. Each atom has three σ-bonds (one with each three neighbours) and one π-bond oriented towards out of the plane. The hexagonal lattice of graphene can be considered as two lattices of interleaving triangular, as illustrated in Fig. 2.3 (Cooper et al., 2012). The bond length of C-C atoms in graphene is approximate 0.142 nm. The stacking of graphene sheets with an interlayer spacing of 0.335 nm forms the graphite. The thickness of graphene is about ~ 0.35 nm, which is 1/200000 times of the diameter of human hair. The graphene has a specific area of 2630 m^2/g, which is much larger than that of carbon nanotubes (CNTs) and carbon black (Bonaccorso et al., 2015).

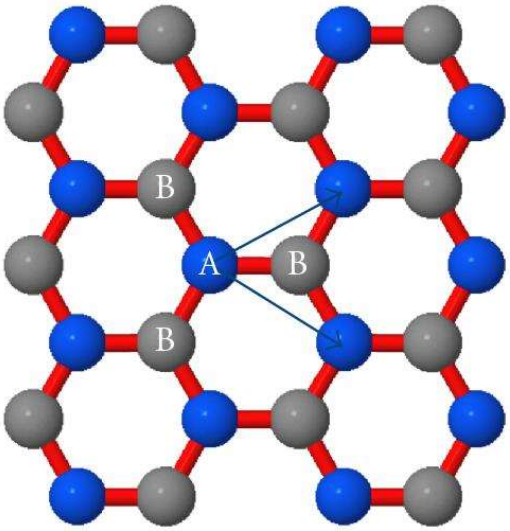

Fig. 2.3 Triangular sublattices of graphene. (Cooper et al., 2012)

Graphene is one of the strongest materials with a very light-weight of 0.77 mg/m^2, which is about 0.001 % of the weight of 1 m^2 of paper. The graphene has a considerably high tensile strength of ~ 130 GPa and Young's modulus (stiffness) of ~ 1TPa (Lee et al., 2008). It is 100 times stronger than the steel of same thickness. The suspended graphene sheets of thickness less than 10 nm have a spring constant of 1-5 N/m with Young's modulus of 0.5 TPa (Frank et al., 2007). Since the graphene is a 2-dimensional layer of carbon, every C atom is available to react chemically from two sides. Defected graphene has more chemical reactivity (Denis and Iribarne, 2013). The burning temperature of graphene is as low as 350 °C (Eftekhari and Jafarkhani, 2013) and it is highly conductive with an electrical conductivity of 10^6 S/m and sheet resistance of 31 Ω/square. Electrons in graphene have ultrahigh mobility of about 2×10^5 cm^2/Vs, which is almost 140 times that of silicon (Zhen and Zhu, 2018). Balandin et al. (2008) reported that the thermal conductivity of graphene is about ten times higher than that of copper at room temperature and is about 5.3×10^3 W/mK. Graphene exhibits unique optical properties, which can be influenced by the thickness of graphene. One atom-thick layer of graphene has a very high optical transparency of 97.7%, which means that graphene absorbs only 2.3% of visible light (Nair et al., 2008). Different layers of graphene exhibit different contrast spectra generated by the reflection of white light (Ni et al., 2007).

Figure 2.4 shows the overview of interactions between graphene and different substrates surfaces such as metals, semiconductors, ceramics, polymers, biomaterials, and liquids. The influence of the substrate on the properties and intended application, including optoelectronics, surface catalysis, anti-friction, superlubricity, coatings, and composites, has also been illustrated in Fig. 2.4. Graphene finds many application in different industries like transport, medicine, electronics, energy, defence, aerospace, and

desalination due to its magical properties. Being very thin and having large specific area, graphene finds its application in battery, super-capacitors and fuel cell, which have light-weight, higher capacity, faster charging, and ability to function under different temperature range. Graphene-reinforced composite materials have potential applications in aerospace, ship-building, manufacturing, construction, mobile and computer accessories, to name a few. Apart from these, graphene has many other promising applications such as anti-corrosion coatings and paints, efficient and precise sensors, functional inks, faster and efficient electronics, flexible displays, efficient solar panels, faster DNA sequencing, drug delivery, and many more.

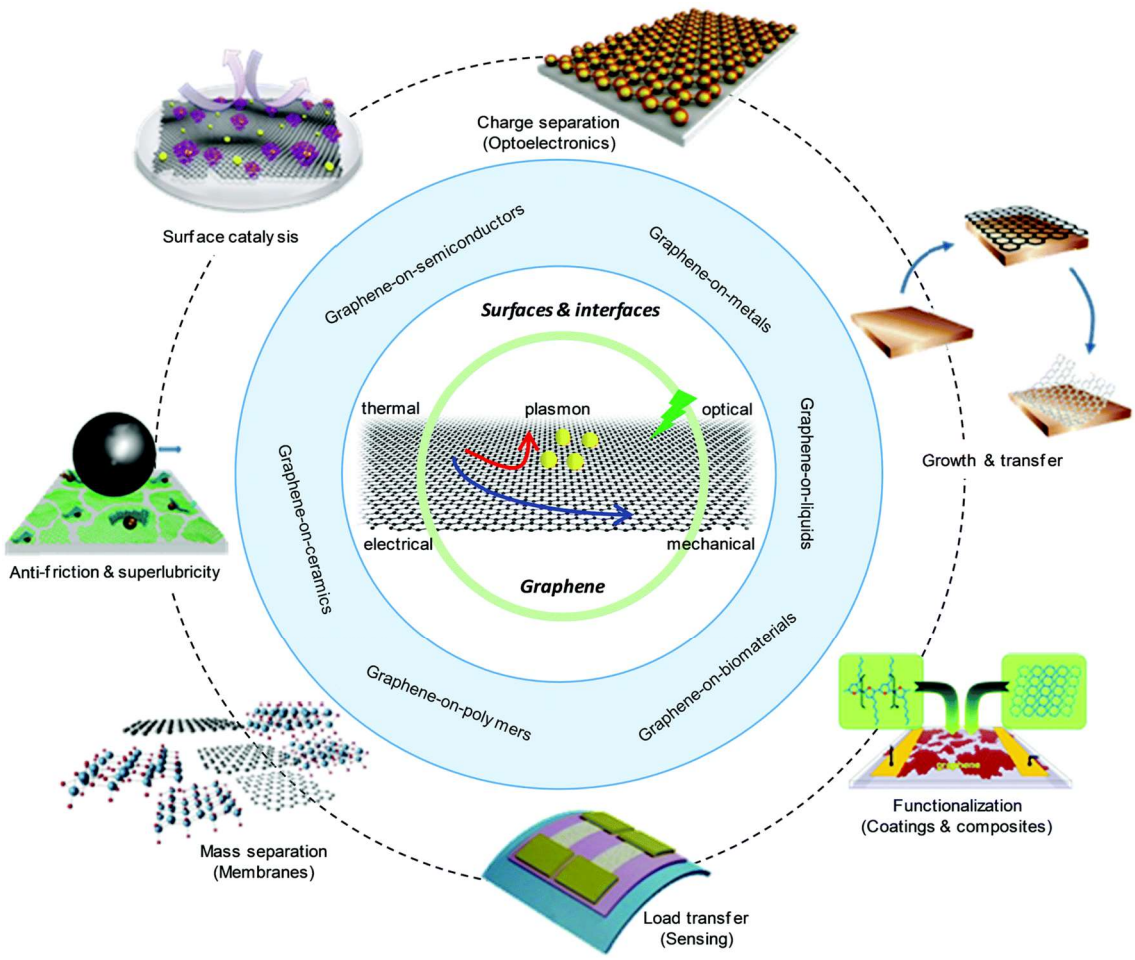

Fig. 2.4 Overview of "graphene-on-surface" systems showing the surface and interface influences and relevant applications. (Zhao et al., 2017)

2.6 METHODS OF GRAPHENE SYNTHESIS

The vast scope of graphene in various applications has motivated researchers from various fields to invent or develop the methods of graphene synthesis. Presently, Top-down (TD) and bottom-up (BU) are two primary approaches to synthesise graphene. In the case of BU, one starts with something smaller and proceeds to make it larger. BU approach consists of graphene synthesis methods such as chemical vapour deposition (CVD), epitaxial growth on silicon carbide, etc. Conversely, TD starts with something larger and proceeds to make it smaller through the removal of the extraneous material (Tour, 2013). TD approach includes the graphene synthesis methods such as unzipping of carbon nanotubes (CNTs), mechanical exfoliation, chemical exfoliation, arc discharge, exfoliation of graphite intercalation compounds (GICs), etc. A broad classification of graphene synthesis method has been presented in Fig. 2.5. Some standard methods of graphene synthesis are presented and discussed in the following sections.

2.6.1 MECHANICAL EXFOLIATION

Geim and Novoselov (2004) isolated a single atomic layer of carbon, i.e., graphene for the first time using the scotch tape method. In this method, graphene was fabricated by repeated peeling of highly oriented pyrolytic graphite with scotch tape, as shown in Fig. 2.6. This method is widely known as a mechanical exfoliation method. It does not require substantial investment or complicated instruments, and the quality is quite good as it originates directly from bulk graphite, but there is a limitation for fabricated graphene size.

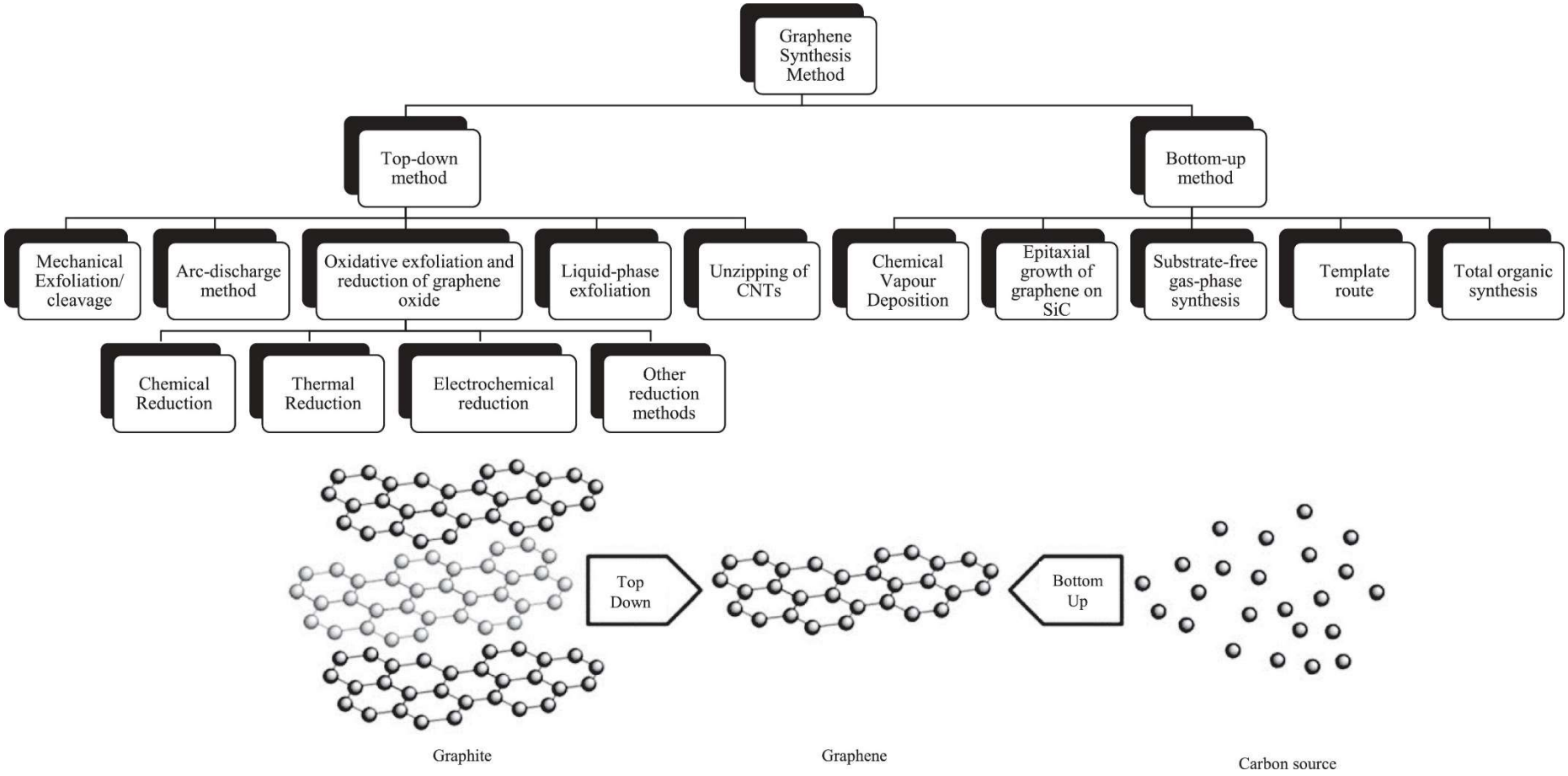

Fig. 2.5 Methods of graphene synthesis. (Lee et al., 2019)

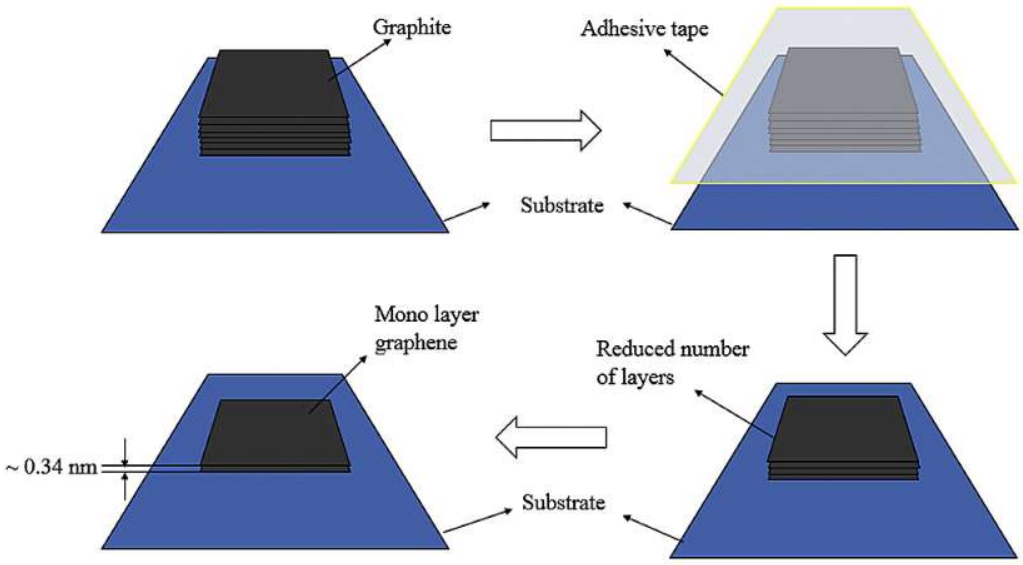

Fig. 2.6 Schematic representation of the mechanical exfoliation of graphene from HOPG using Scotch tape. (Dasari et al., 2017)

2.6.2 CHEMICAL EXFOLIATION

The chemical exfoliation method of producing graphene from graphite and graphite intercalation compounds is an alternative approach to mechanical exfoliation. Chemical exfoliation is a two-step process involving (i) an increase in interlayer spacing to form intercalated compounds by reducing the interlayer van der Waals forces, (ii) exfoliation to form single to few-layer graphene by sonication or rapid heating (Bhuyan et al., 2016). Schematic of thermal expansion mechanism of graphite/graphite oxide to produce functionalised graphene sheets has been presented in Fig. 2.7.

2.6.3 ELECTROCHEMICAL EXFOLIATION OF GRAPHENE

Electrochemical exfoliation of graphite involves the intercalation of voltage-driven ionic species into graphite to increase the interlayer distance (Achee et al., 2018).

Rao et al. (2014) used sodium hydroxide/hydrogen peroxide/water ($NaOH/H_2O_2/H_2O$) system for electrochemical exfoliation (shown in Fig. 2.8) of graphite to produce high-quality few-layer graphene with 95% yield. However, the disintegration of graphite with the progress of the method is the major problem associated with the electrochemical exfoliation of graphene.

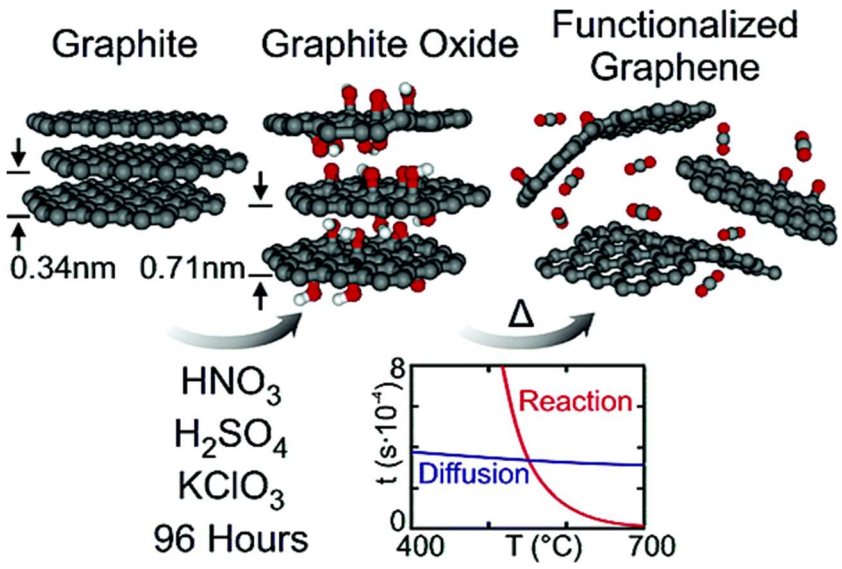

Fig. 2.7 Schematic of thermal expansion mechanism of graphite/graphite oxide to produce functionalised graphene sheets. (McAllister et al., 2007)

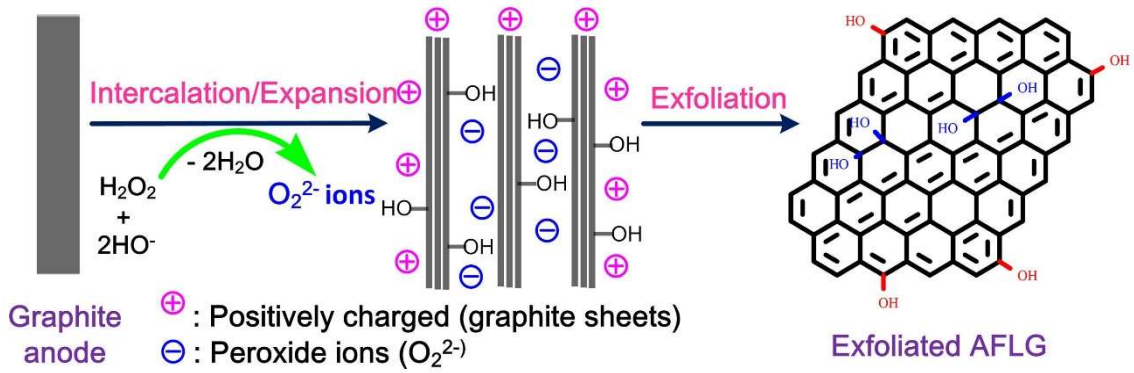

Fig. 2.8 Schematics of the electrochemical exfoliation mechanism of graphene production. (Rao et al., 2014)

2.6.4 EPITAXIAL GROWTH ON SILICON CARBIDE (SiC)

Graphene can be epitaxially grown by annealing of silicon carbide at a high temperature in the vacuum atmosphere through the sublimation of Si from the SiC surface as reported by Sutter (2009). When SiC substrates are annealed at a high temperature, the desorbtion of Si from the substrate occurs, leaving behind carbon atoms and thus constituting the graphene, as shown in Fig. 2.9 (Hibino et al., 2010). Graphene with different layers can be grown under the controlled condition of temperature and pressure. The number of synthesised graphene layers can be measured from quantised oscillations of reflectivity of low-energy electrons from graphitised SiC (0001) (Hibino et al., 2008). Lattice constant mismatch and the possibility of introduction of various defects due to differences in coefficient of thermal expansion are the major problems associated with the production of graphene using this method. Also, it is hard to transfer graphene produced by the graphitisation of SiC to an arbitrary substrate.

2.6.5 UNZIPPING OF CARBON NANOTUBES

Since carbon nanotubes (CNTs) are made of rolled graphene sheets, the graphene can also be obtained from cutting and unravelling of CNTs, as shown in Fig. 2.10. Several methods have been proposed for the unzipping of CNTs such as chemical oxidation, electron beam steam and plasma etching, hydrothermal, electrochemical, intercalation, etc. (Mondal et al., 2018). After unzipping, single-walled CNT and multi-walled CNTs produce single-layer and multi-layer graphene, respectively.

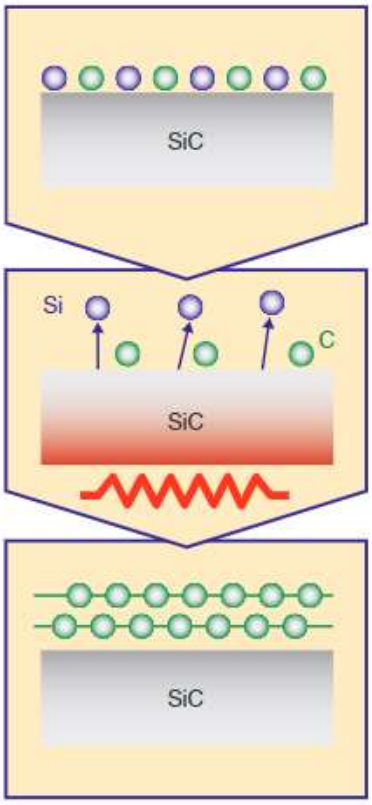

Fig. 2.9 Schematic illustration of the thermal decomposition method. (Hibino et al., 2010)

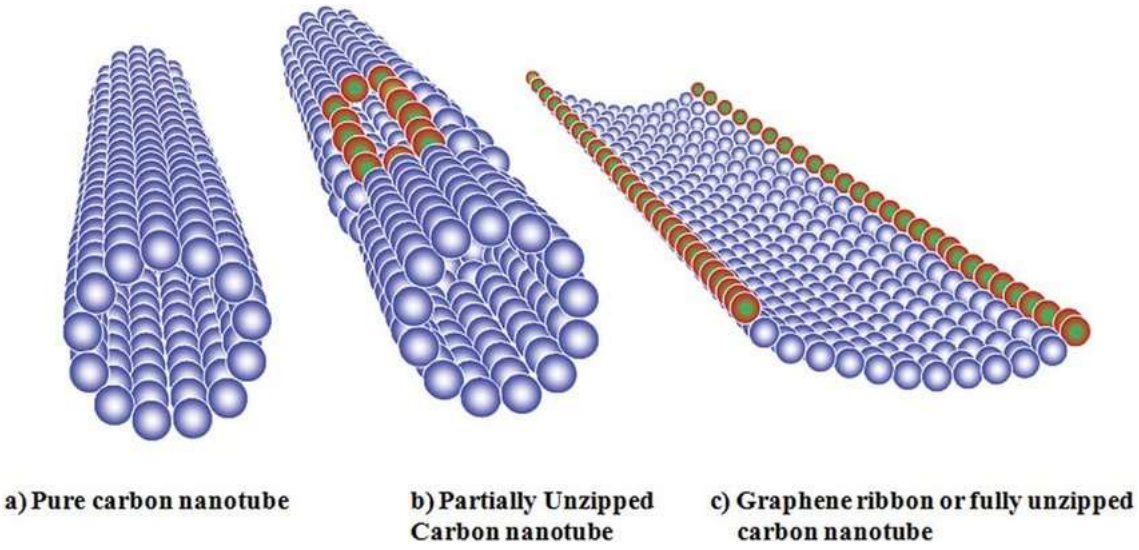

Fig. 2.10 A schematic of the unzipping of carbon nanotubes to form graphene (Sivaraman et al., 2015).

2.6.6 CHEMICAL VAPOUR DEPOSITION

The chemical vapour deposition method of graphene synthesis can produce high-quality graphene over a large area. CVD involves the deposition of gaseous precursor onto the substrate. The gases (precursor and carrier) are combined in a chamber maintained at a certain temperature and pressure. The reaction occurs on the substrate surface to form material (graphene) film, and the waste gases are pumped out of reaction temperature. Figure 2.11 shows scalability, cost, and graphene quality trends for different manufacturing techniques of graphene synthesis.

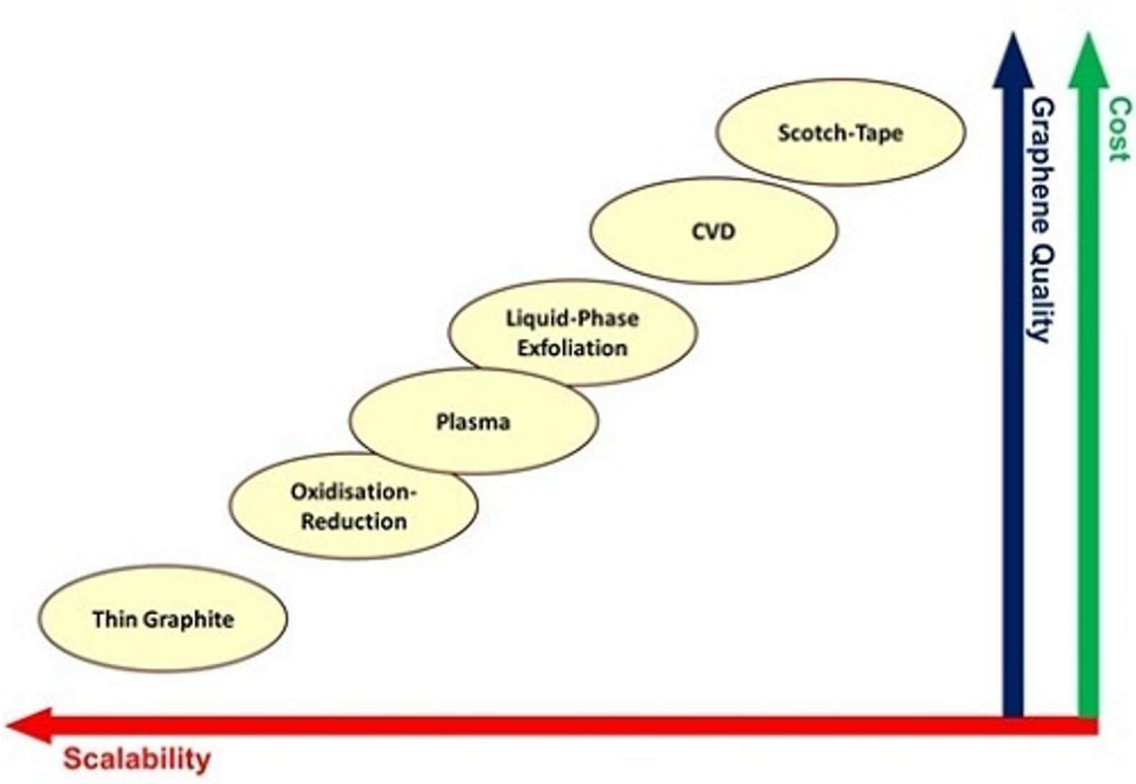

Fig. 2.11 Scalability, cost, and graphene quality trends for different manufacturing techniques. (Ghaffarzadeh, 2012)

2.7 CHEMICAL VAPOUR DEPOSITION OF GRAPHENE

Although mechanical exfoliation does not require substantial investment or complicated instruments, but there is a limitation for fabricated graphene size. To avoid the limitation of the size of graphene for large-area applications, graphene has been fabricated by other methods such as chemical methods, ultrahigh vacuum annealing of single-crystal SiC (0001), chemical vapour deposition, and reduction of graphene oxide films deposited by the liquid suspension. Among all known methods of graphene production, the chemical vapour deposition is found to be the most suitable method for growing graphene with high quality and controlled nucleation over a large area among all graphene synthesis processes as reported by Li et al. (2011). The graphene is synthesised through chemical vapour deposition by thermal decomposition of carbon-based precursors such as ethanol, methane, ethylene, acetylene. For CVD growth of graphene on a surface, carbon atoms surface segregation, and carbon atoms surface deposition are the two well-recognised mechanisms as indicated by Li et al. (2009) and Al-Shurman and Naseem (2014).

In the case of carbon atoms surface segregation, the carbon atoms first diffuse into the surface at high temperature and later, precipitate on the surface during the cooling (e.g., Ni). However, for the carbon atoms surface deposition, carbon atoms are deposited directly over the surface without any diffusion or precipitation (e.g., Cu). A typical schematic diagram for chemical vapour deposition for graphene is presented in Fig. 2.12.

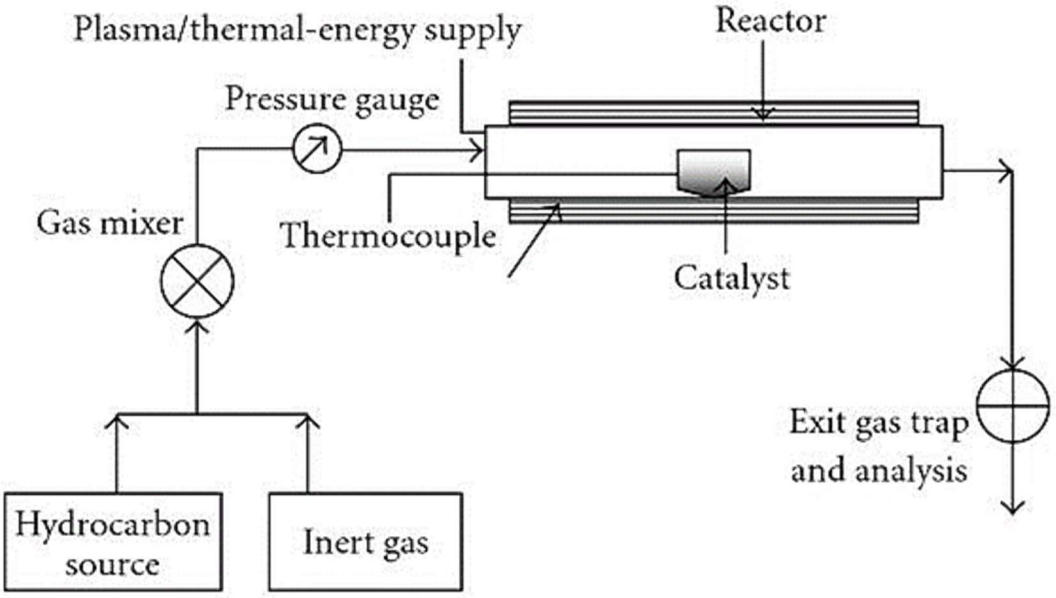

Fig. 2.12 Schematic diagram of a CVD process. (Shivkumar et al., 2010)

2.7.1 TYPES OF CVD PROCESS

Although the CVD process of synthesising graphene can be classified in various ways such as operating pressure conditions (atmospheric, low-pressure, ultra-high vacuum), type of substrate heating (hot-wall and cold-wall), and plasma methods (plasma-enhanced, low energy plasma-enhanced, remote plasma-enhanced, microwave plasma-assisted), however, the classification based on operating pressure is the most popular. Based on the operating pressure, the CVD processes can be divided into three categories, as discussed below:

i. **Atmospheric pressure CVD (APCVD):** APCVD is the CVD procedure carried out at atmospheric pressure. Bhaviripudi et al. (2010) synthesised graphene on Cu catalyst under APCVD conditions using different compositions of methane gas and found a change in growth from monolayer graphene (at low methane

concentrations) to multilayer domains on a monolayer (at higher methane concentrations).

ii. **Low-pressure CVD (LPCVD):** LPCVD is the CVD process carried out at a pressure lower than atmospheric, which prevents unwanted gas-phase reactions and produces more uniform coatings than that produced by APCVD. The importance of this method lies in the fact that it operates at low pressure of the order of few torrs due to which the velocity of mass transport of the source gas gets reduced which results in the larger exposure of the substrate to the gas leading to better and homogeneous deposition.

iii. **Ultra-high vacuum CVD (UHVCVD):** UHVCVD is the CVD procedure carried out under extremely lower pressures of the order of 10^{-6} Pa. Mueller et al. (2014) synthesised monolayer graphene on polycrystalline copper via UHVCVD using acetylene and hydrogen and reported that the graphene growth is self-limiting with quality comparable to that of APCVD/LPCVD.

2.7.2 TRANSITION METALS FOR CVD GROWTH OF GRAPHENE

Several researchers (Vanin et al., 2010; Bartelt and McCarty, 2012; Batzill, 2012; Dedkov and Voloshina, 2015) have reported that various metal catalysts and alloys, help in the decomposition of carbon from its sources to synthesise graphene on the substrate. The mechanism of graphene growth and its quality are dependent on transition metal. Batzill (2012) has summarised the interaction between graphene and transition metals and a schematic diagram for the same is presented Fig. 2.13, where “S” and “M” stand for graphene with single or multiple rotational domains, respectively, “d” indicates

the separation distance (Å) of graphene and metal, "c" is the corrugation of graphene sheet in Å, π stands for the amount of shift of π-band. The yellow and red colours represent the elements having weak and strong interaction with graphene, respectively. However, the graphene can also be grown on bulk carbides labelled in blue colour in Fig. 2.13. Based on the interaction between graphene and transition metals, graphene may be grown either by physisorption or chemisorption. Cu and Ni are the two most widely used transition metal for CVD synthesis of graphene.

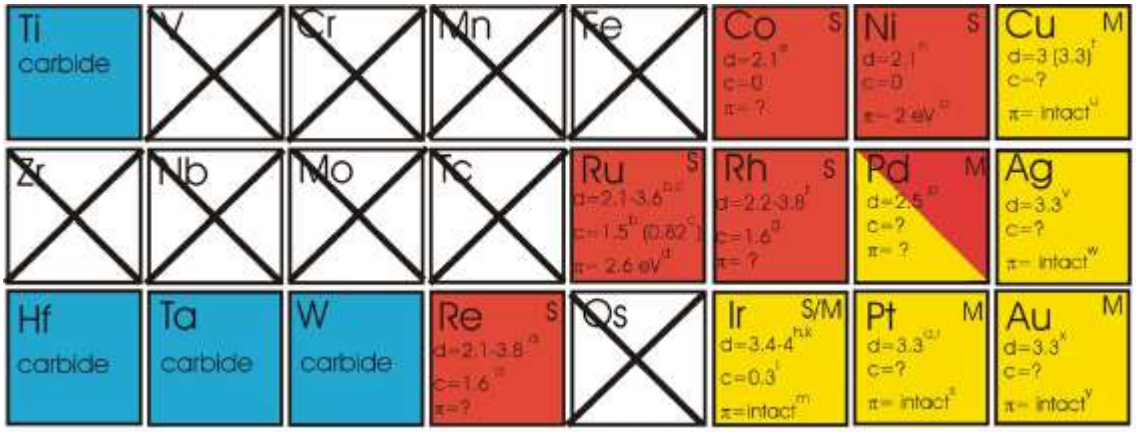

Fig. 2.13 Summarised representation of the interaction between graphene and transition metals. (Batzill, 2012)

In the case of copper, the formation of graphene is due to direct adsorption of carbon on the copper surface, since it has low solubility of carbon (Li et al., 2009; Zhao et al., 2013). The mechanism of graphene growth on copper has been illustrated in Fig. 2.14, which shows that the growth is self-limited on the copper surface due to low carbon solubility in copper. Baraton et al. (2011) investigated the growth of graphitic materials on nickel using CVD and reported that the graphene growth on nickel consists of the decomposition of the carbon-based precursor at high growth temperature, diffusion of

carbon atoms into the nickel due to substantial solubility of graphene in nickel, followed by segregation over the surface during cooling. Few- to multi-layer graphene has been produced usually over nickel due to the high solubility of carbon.

Yu et al. (2008) reported the graphene growth on nickel surface under the ambient pressure by allowing the decomposition of hydrocarbon gases into carbon atoms and hydrogen at a high temperature (1000 ℃) over the nickel surface for 20 min. The carbon atoms get dissolved into the nickel forming a solid solution, and finally, carbon is segregated over the nickel surface during the cooling as shown in Fig. 2.15, the segregation behaviour being dependent on the rate of cooling. Several layers of graphene could be synthesised under controlled cooling rate. An extremely fast cooling rate results in the formation of graphite, indicating that more number of carbon atoms segregate at the surface in short time as they do not get enough time to reach a state with good crystallinity. On the other hand, a slow cooling rate allows the diffusion of carbon atoms into the surface for sufficient time, and thus, reduces the number of segregated carbon atoms. The fast or medium cooling rates have been reported to be the best for synthesising few-layer graphene. It has also been reported that the graphene growth on nickel is faster than that on copper (Baraton et al., 2011; Reina et al., 2008).

In a study, Pu et al. (2015) reported that the plating of nickel on steel surface reduced the formation of metal carbide as it acts as a barrier layer and lessens the carbon diffusion on the steel. At the same time, high carbon solubility and high catalytic activity of nickel lead to the formation of multi-layer graphene due to increased pyrolysis of carbon source. For these reasons, nickel has been and is being used widely as a metal catalyst for CVD growth of graphene.

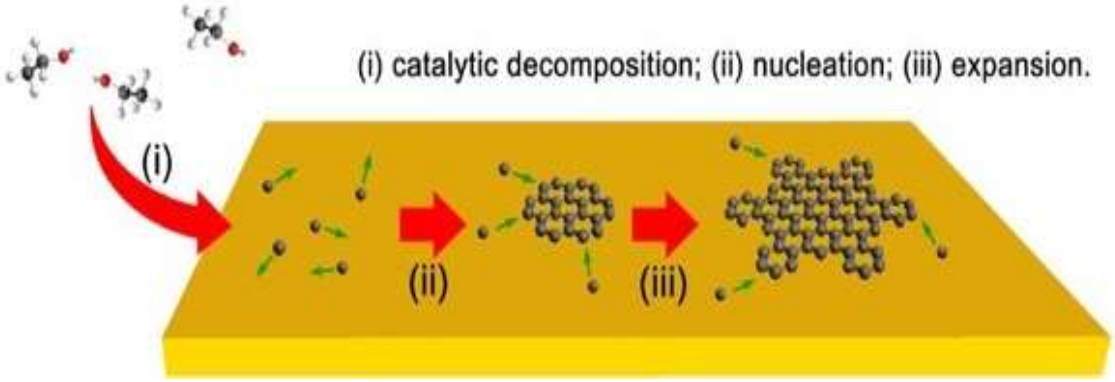

Fig. 2.14 Schematic of CVD graphene grown on Cu foil. (Zhao et al., 2013)

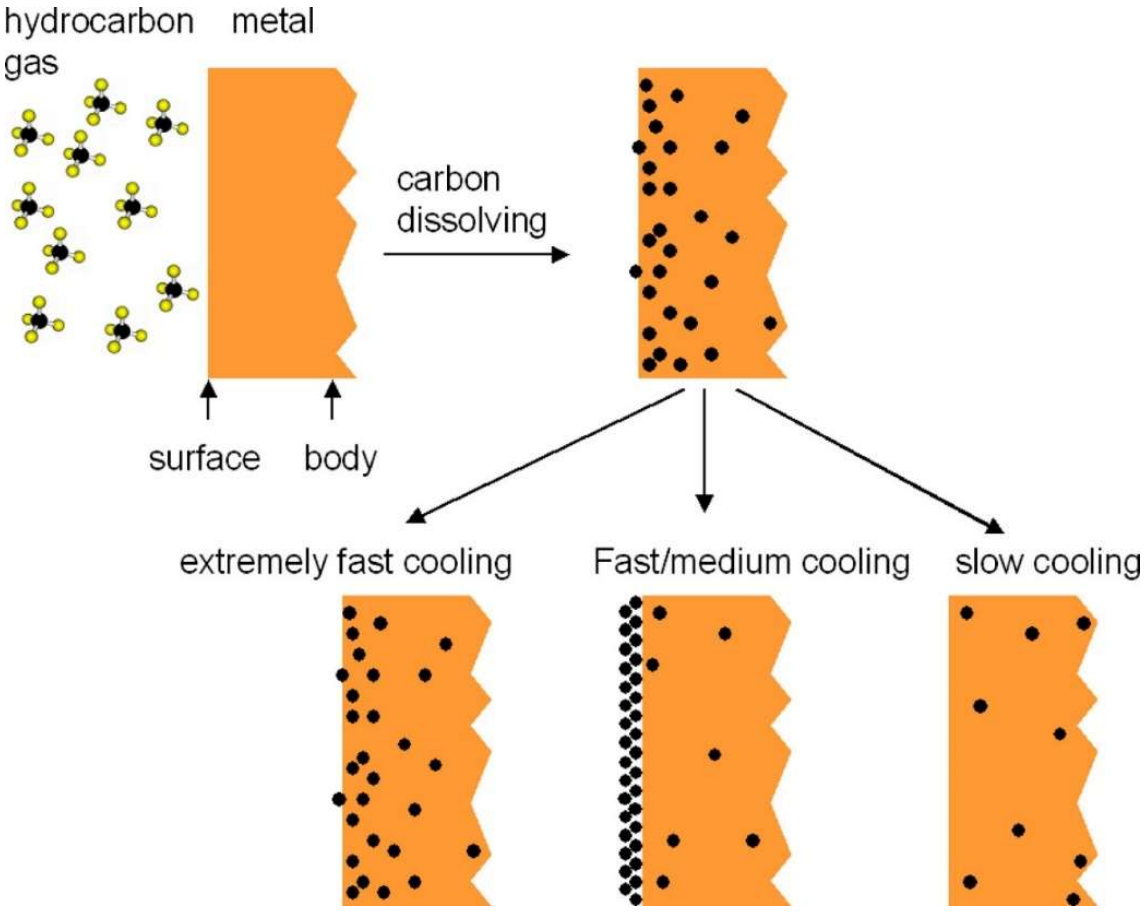

Fig. 2.15 Illustration of carbon segregation at the metal surface with high carbon solubility such as nickel. (Yu et al., 2008)

2.7.3 PARAMETERS AFFECTING THE CVD GROWTH OF GRAPHENE

It has been reported by Liu et al. (2010) and Baraton et al. (2011) that the graphene growth is affected by various parameters such as growth temperature, type of hydrocarbon source and its flow rate, reaction time, cooling rate, substrate material (quality, structure, carbon solubility) etc.

Liu et al. (2010) studied the effect of growth temperatures (850 to 1000 ℃), reaction times (50 to 120 s) and cooling rates (7 to 25 ℃/min) on CVD growth of graphene on a SiO_2/Si substrate covered with a nickel film and reported that the most uniform, large area and single-layer graphene covering the 50 % area of 1-inch substrate can be achieved at 900 ℃ for a growth time of 50 s under the fastest cooling rate of 25 ℃/min.

John et al. (2011) reported a direct thermal chemical vapour deposition method to synthesise single- and few-layer graphene on SS 304 using ethanol and revealed that the chemical species presented on the surface might enhance or retard the graphene growth on the steel. It has been demonstrated that the presence of FeO enhances the graphene growth, while the excess Cr and Mn hinder the graphene growth.

Dathbun and Chaisitsak (2013) successfully synthesised the high-quality graphene on copper by CVD using ethanol and studied the effects of growth temperatures (650 to 950 ℃), reaction times (5 to 50 min) and cooling rates (41, 80, 293 ℃/min) to obtain the best conditions of graphene growth. On the basis of the Raman spectra at various temperatures, it has been concluded that the high-quality graphene could be grown at a growth temperature of 850 ℃. A lower growth temperature leads to a decrease in graphene quality due to poor graphitisation at the lower temperature, while the higher

temperature causes the evaporation of copper foil. For different reaction times, the highest I_{2D}/I_G and lowest I_D/I_G ratio have been observed for a reaction time of 30 min, indicating the excellent coverage of graphene over the surface with a low level of defects. It was reported that the cooling rate has no significant effect on the number of graphene layers. However, under a faster cooling rate, the graphene with a large domain size could be synthesised.

Chen and Hsieh (2015) studied the effect of growth temperatures (500, 600, 700, 800 and 900 °C) and acetylene flow rates (6, 12, 24 and 36 sccm) on synthesised graphene by thermal chemical vapour deposition on nickel foil and reported that the graphene could not be synthesised below a temperature of 600 °C. However, the quality of synthesised graphene was inferior at 600 °C compared to that grown at higher processing temperatures. The authors varied the acetylene flow rate to improve the quality of low-temperature-synthesised graphene and reported that a moderate flow rate (6 sccm) is the best to synthesise a comparatively high- quality graphene.

Lavin-Lopez et al. (2015) conducted a study with the aim to optimise the graphene growth over polycrystalline nickel using CH_4 as a precursor and H_2 and N_2 as the carrier gases in a CVD system and investigated the effects of reaction temperatures (900 to 1050 °C), CH_4/H_2 flow rate ratios (0.4 to 0.07 v/v) in the feed and reaction times (30 to 900 s). The authors synthesised different types (monolayer, bilayer, few-layer, and multi-layer) of graphene films for each condition and obtained the highest thickness value with 77% of nickel surface coverage with monolayer graphene for the temperature, CH_4/H_2 flow rate ratio and reaction time of 980 °C, 0.07 v/v and 60 seconds, respectively. Lavin-Lopez et al. (2016) further optimised the total gas flow ($CH_4 + H_2$) for different reaction times and reported that a total gas flow of 80 NmL/min for a reaction time of 1

min could achieve the maximum thickness value with 80% of nickel surface coverage with monolayer graphene.

Ghaemi et al. (2016) demonstrated the CVD growth of different layers of graphene on stainless steel coated with Cu catalyst for different reaction temperatures (950, 1000, and 1050 °C) and run times (10 to 50 min) using acetylene (50 sccm) as a carbon source and H_2 and N_2 as carrier gases. An increase in the amount of graphene and a decrease in the number of graphene layers have been reported with increasing temperature. However, both the amount of graphene and the number of graphene layers increased with an increase in reaction time.

2.8 ROLE OF GRAPHENE IN TRIBOLOGY

The coating of carbonaceous materials to improve the different properties has been famous for decades. Among all carbon materials, low interlayer shear stress, high chemical inertness, atomically smooth surface, and excellent strength of graphene are the desirable properties from the tribological point of view. Graphene, as a solid lubricant reduces the friction forces between the contact surfaces on nano-, micro- and macro-scale while protecting the coated surface. The solid lubrication effect of graphene is due to its lamellar structure with low interlayer shear strength. Tribology of graphene involves its use in the form of coatings, additive in lubricants, and reinforcement in the composites.

2.9 FRICTION AND WEAR OF GRAPHENE COATINGS

Several researchers (Lee et al., 2010; Kim et al., 2011; Berman et al., 2013, 2013, 2014; Chen et al., 2017; Bhowmick et al., 2015; Yildiz et al., 2018, Chen et al.,

2019) have investigated the tribological behaviour of graphene coating on various substrates under a range of sliding conditions.

Lee et al. (2010) deposited graphene onto SiO_2/Si and compared the frictional behaviour of atomically thin sheets of graphene to bulk graphite at the nanoscale employing silicon AFM probes in contact mode at an applied force of 1 nN. The friction trends were recorded from 1 to 10 μm/s and found to be independent of speed. The authors reported a decrease in friction with increasing thickness and a similar friction behaviour for four-layer graphene sheets and bulk graphite.

Kim et al. (2011) synthesised the monolayer and multilayer graphene on Cu and Ni, respectively, and transferred them on a SiO_2/Si and investigated their adhesion and frictional characteristics of both the transferred and untransferred graphene by carrying out friction tests using a micro-tribometer against the fused silica lens (radius of curvature 25.8 mm). For each set of friction test, the load was increased from 5 to 70 mN with a sliding speed of 50 μm/s for a sliding distance of 1000 μm. The authors reported a significant reduction in the friction coefficient after the transfer of graphene on SiO_2/Si and concluded that Ni-grown graphene transfer on SiO_2/Si had a lower coefficient of friction than that transferred Cu-grown graphene and attributed it to the increased thickness of graphene.

Berman et al. (2013, 2013) studied friction and wear for self-mated 440C steel lubricated with solution-processed graphene (SPG) in the dry nitrogen and air at room temperature by conducting under a normal load of 2 N and sliding speed of 60 rpm against a ball of 9.5 mm diameter with a track radius of 15 mm. Few drops of SPG were applied on the polished steel surfaces and then, dried in a nitrogen atmosphere to prevent

oxidation of graphene so that ethanol was evaporated from SPG. The results of tribological tests revealed a six times reduction in friction coefficient and 3-4 orders reduction in wear volume in comparison to those observed for bare steel under the tested conditions in dry nitrogen and air, respectively. The observed reduction has been attributed to the low shear and highly protective nature of graphene over the surface.

In another study, Berman et al. (2014) demonstrated the macroscale wear resistance of one atom thick graphene coating for the steel against steel tribo-pair. The tests were conducted in a dry hydrogen atmosphere under a normal load of 1 N and a sliding speed of 60 rpm with varying track radius from 5 to 15 mm. It was found that the one atom thick graphene can sustain even after 6400 cycles under a contact pressure of 0.5 GPa in hydrogen atmosphere without any evidence of measurable wear. Conversely, monolayer graphene was worn out after several hundred cycles in a dry nitrogen environment.

Bhowmick et al. (2015) examined the role of humidity on the friction behaviour of multilayer graphene grown on nickel. The rotating sliding tests were conducted in the air with different relative humidity (10-45 % RH) and dry nitrogen (0 % RH) using pin-on-disk configuration against Ti-6Al-4V ball. The sliding tests were conducted at a constant speed of 0.05 m/s under a fixed normal load of 1 N. The minimum friction coefficient of 0.11 was observed for a relative humidity of 45% due to the availability of more number of H and OH molecules on worn graphene and transfer layers, which led to repulsive attractions between H-H, OH-OH, and H-OH to reduce the friction force.

Shi et al. (2016) prepared parallel microgrooves with different groove area ratios (14, 35 and 56 %) on the M2 steel surfaces using laser texturing and spread graphene-containing ethanol solution over it to study the synergetic effect texturing and few-layer graphene on tribological properties of M2 steel surfaces. Reciprocating sliding tests were conducted in the air against AISI 52100 ball at a normal load of 0.5 N with a sliding velocity of 3 mm/s. It was concluded that the groove served as a reservoir of graphene and enhanced wear resistance, especially for a groove area ratio of 35 % due to the entrapment of wear debris in grooves and the formation of a protective layer of carbon over the contact surfaces.

Chen et al. (2017) demonstrated the tribological behaviour of graphene prepared by electrophoretic deposition on micro-crystalline diamond (MCD) surface sliding against Si_3N_4 under a range of normal loads (4 to 10 N). The reciprocating friction tests were conducted against silicon nitride ball in ambient condition with a skidding frequency of 2 Hz over a stroke of 10 mm. A friction coefficient in the range of 0.07-0.09 was achieved, indicating no discernible dependence on the applied load.

Hong et al. (2018) synthesised the graphene coatings on silicon wafer by electrophoretic deposition under different combinations of deposition voltage, deposition time, and concertation of graphene in suspension and investigated their frictional behaviour under reciprocating sliding at different loads (1 to 9 N) against a 4 mm diameter silicon nitride ball with a sliding frequency of 2 Hz over a stroke length of 6 mm in ambient condition. It was observed that graphene coating could reduce friction coefficient by over 80 % than that of bare Si under a load of 1 N.

To evaluate the wear behaviour of monolayer graphene, Huang et al. (2017) carried out reciprocating wear tests at microscale against BK7 glass plano-convex lens in ambient conditions (35% ≤ RH ≤ 46%) and nitrogen environment (RH ≤ 5%). BK7 glass lens of 5mm radius of curvature was selected as a counterface. The tests were conducted with normal load ranging 50 to 80 μN over the sliding length of 50 and 100 μm. It was suggested that the wear was absent up to a critical load after that friction started to increase gradually due to the wear of graphene. The friction behaviour of monolayer graphene at macroscale was similar to graphite and was best in a humid environment (RH – 40 %) than that in a dry environment (RH ≤ 5%).

Roamani et al. (2017) investigated the friction behaviour of the graphene grown at different pressures of 200 and 400 mTorr on API X80 steel against stainless steel ball under reciprocating sliding. The tests were conducted under normal loads of 0.3 and 1 N with a sliding speed of 10 mm/s over a sliding amplitude of 10 mm. It was revealed that even with the partial coverage of graphene, the sample coated at 200 mTorr had shown the best and almost constant friction behaviour with a coefficient of friction of ~ 0.15 due to presence of the graphitic structure on the contact surfaces, which reduced the interfacial adhesion as well as shear strength.

Zheng et al. (2017) investigated the friction behaviour of graphene on the plasma-treated substrate (SiO_2). Friction tests were conducted with a scanning speed of 600 nm/s. Plasma treatment was utilised to enhance the adhesion of graphene on the substrate, and it was found that the longer duration of plasma treatment resulted in better adhesion between the graphene and substrate, and also minimised the effect of thickness on friction force. However, it was observed that the friction force of plasma-treated SiO_2 increased with increasing time of plasma treatment.

Sun et al. (2019) reported the effects of load (1 to 5 N) and sliding speed (20 to 240 rpm) on friction and wear behaviour of multilayer graphene (MLG) coating on nickel foil. The stainless steel (440C) ball of 6 mm diameter was used as counterface for a test duration of 3600 cycles. It has been found that under low normal loads (1-3 N) and low sliding speeds (30-120 rpm), the multilayer graphene can provide excellent tribological properties for more than 3600 cycles with a coefficient of friction of 0.06. However, with increased load and sliding speed, it was observed that the graphene coating failed after limited sliding cycles and the coefficient of friction increased due to breakdown of MLG coating

2.10 TRIBOLOGY OF GRAPHENE AS AN ADDITIVE

Apart from being used as solid lubricant coating, graphene and its derivatives may be used as additives in traditional lubricants due to their lubricious nature. The utilisation of graphene as an additive has attracted the attention of researchers/tribologists across the globe during the last few years. Several studies have demonstrated the utility of graphene as an additive in improving tribological performance. The chemically inert nature of pristine graphene makes it quite challenging to uniformly disperse or dissolve in lubricants. So, physical and chemical modifications are required to enhance the solubility and dispersibility of graphene (Wang et al., 2009). A stable dispersion of graphene in lubricants such as oils, water, and other fluids as an additive has been reported by many researchers (Zhang et al., 2011; Kinoshita et al. , 2014; Fan and Wang, 2015; Sur et al., 2016; Qamar et al., 2019).

Zhang et al. (2011) modified the liquid phase exfoliated graphene sheets by oleic acid and dispersed its different concentrations (0.02-5 wt. %) uniformly by ultra-sonication in PAO 9. A four-ball tribometer was employed for investigating the tribological behaviour. The tribological tests were conducted using GCr15 ball of 12.7 mm diameter under a load of 400 N with a speed of 1450 rpm, and it was reported that the graphene concentration of 0.02 and 0.06 wt. % showed enhanced friction and anti-wear performance, respectively. Compared to pure PAO 9, the mentioned graphene concentration was able to reduce the friction coefficient by 17% and wear scar diameter by 14%.

Fan and Wang (2015) investigated the tribological properties of modified graphene oxide (MGO) and modified graphene (MG) as additive in multialkylated cyclopentanes (MACs) by carrying out reciprocating sliding tests using self mated AISI 52100 tribo-pair with a ball-on-block configuration at a normal load of 100 N and sliding frequency of 25 Hz for a duration of 1 hour and reported a considerable improvement in anti-friction and anti-wear abilities, attributing it to the synergetic effect of physically adsorbed film and ILs-containing graphene-rich film formed due to tribo-chemical reaction.

Azman et al. (2016) added different concentrations of graphene nanoplatelets (GNPs) in polualphaolefin (PAO 10) blended with palm-oil trimethylopropane (TMP) ester and conducted tribological tests in a four-ball tester using AISI 52100 steel ball of 12.7 mm diameter under a load of 392 N with 1200 rpm sliding speed at room temperature. A concentration of 0.05 wt. % of GNPs has been reported to be optimum concentration based on the friction coefficient and wear scar diameter. It has also been concluded that a concentration higher than 0.05 wt. % lead to rapid collisions between

GNPs and formed large lumps of GNPs, which acted as an abrasive body and increased the wear loss.

Guo and Zhang (2016) studied the friction and wear behaviour of multi-layer graphene as additives of polyalphaolefin (PAO 2) using a four-ball tester for steel-steel contacts under different normal loads (120-400 N) and different rotation speeds (100-400 rpm). It was reported that 0.05 wt. % is the favourable concentration of multi-layer graphene in PAO 2 since it shows the better dispersibility and enhanced tribological behaviour by reducing the friction coefficient and wear scar diameter under the conditions used for the study. The improved performance has been attributed to the formation of a thin tribo-layer on the surface, which inhibited the direct contact between the mating bodies.

Considering the environmental and economic concerns, the use of water as a base lubricant is getting the attention of the researchers worldwide. The use of water in place of traditional lubricants has the potential to save huge costs associated with the use and disposal of lubricants. Several studies (Kinoshita et al., 2014; Elomaa et al., 2015; Kim and Kim, 2015; Xie et al., 2018) related to the use of graphene or its derivatives as lubricant additive in water have been reported. Kinoshita et al. (2014) performed reciprocating tests under a load of 1.88 N with the sliding frequency of 5 Hz over a stroke of 2.5 mm and achieved a low friction coefficient 0.05 with graphene oxide-water dispersion used a lubricant for WC ball-SS304 plate tribo-systems without noticeable wear even after 60,000 cycles. The enhanced tribological performance has been ascribed to the formation of protective coatings on the surfaces of the ball and plate due to the adsorption of graphene oxide sheets.

Elomaa et al. (2015) investigated the friction and wear behaviour of different concentrations (up to 2 wt. %) of graphene oxide (GO) in water for a tribo-pair of diamond-like carbon and stainless steel under a normal load of 10 N and a sliding speed of 0.03 m/s. The authors obtained a coefficient of friction of ~ 0.06 for 1 wt. % of GO in water and attributed it to the formation of a lubricating layer on the ball due to embedding of GO sheets. However, they also reported an increase in wear rate with increasing concentration of graphene oxide.

Kim and Kim (2015) studied the tribological performance of stainless steel (SS) plate against reduced graphene oxide (rGO) coated SS ball with water as a lubricant. Reciprocating sliding tests were performed under different normal loads of 50, 100, 150, 200 mN with a sliding speed of 4 mm/s over a stroke length of 2 mm. It was reported that for a normal load of 50 mN, a friction coefficient as low as ~0.12 could be maintained over 1,00,000 cycles for rGO coated SS ball against SS plate steel under the water lubrication. The wear rate of the SS plate used against the rGO coated ball was found to be three times lower than that used against the uncoated ball in oil lubrication.

Liang et al. (2016) investigated the tribological performance of in-situ exfoliated graphene as additive in the water on steel (GCr15)-steel (GCr15) contact pair by carrying out friction and wear tests at normal loads ranging from 2 to 15 N with speeds from 60 to 240 rpm and found that a graphene tribo-layer forms at the contact zone of sliding surface which causes a reduction of 81.3 % and 61.8 % in the friction coefficient and wear scar diameter, compared to deionised (DI) water. It has further been reported that in-situ exfoliated graphene in water provides better tribological properties in comparison to the graphene oxide of equal concentration in DI water.

Yang et al. (2017) synthesised the liquid-like graphene by grafting of amino-terminated block copolymer on the graphene surface and dissolved it into deionised water with varying concentrations. The 440-C chromium steel ball was used against a 45# steel with a rotating speed of 100 rpm under a normal load of 50 N to investigate the friction and wear behaviour. It was reported that the 50 mg/ml concentration of liquid-like graphene in water could lower the friction coefficient and wear rate by 53 % and 91 % compared to water, respectively. The observed behaviour has been explained on the basis of the formation of composite tribo-film over the steel surface by electrostatic adsorbtion and rearrangement of graphene molecules.

Xie et al. (2018) investigated the friction and wear behaviour of different concentrations of graphene and graphene oxide (GO) in water-based lubricant additives by carrying out the experiments under different loads (1, 3, 5, and 8 N) with sliding speed of 0.08 m/s over a stoke length of 6 mm. Out of all selected concentrations (0.2, 0.5, 0.7 and 1.0 wt. %) in water, the best tribological performance of magnesium alloy plate against steel ball was obtained at a concentration of 0.5 wt.% for graphene as well as for graphene oxide under reciprocating sliding at a load of 3N and sliding speed of 0.08 m/s. The tribological behaviour of graphene oxide-based lubricants was found to be superior to that of graphene due to strong affinity between graphene oxide sheets and magnesium alloy, excellent dispersion of graphene oxide in water and strong wetting of graphene oxide nanofluids on the surface of magnesium alloy. The friction coefficients and wear rates for graphene oxide nanofluids were reported to be almost constant at all the test loads. However, increasing trends of friction coefficient as well as of wear rate were found for graphene nanofluids with the load.

2.11 FORMULATION OF THE PROBLEM

From the above review of the available literature, it is observed that very limited work has been done on the synthesis and tribological behaviour of graphene coating synthesised by CVD. Most of the tribological studies have been carried out with either solution-processed graphene coating or transferred graphene coatings on steel. To the best of our knowledge, investigations on the direct growth of graphene on bearing steel and its tribological studies have not been reported in any literature so far. However, there is ample scope for studying the possibility of synthesising graphene by direct thermal chemical vapour deposition on steel and examining its friction and wear performance under dry sliding. On the other hand, several studies concerning tribological behaviour of graphene and its derivatives (especially graphene oxide) as additives in oil or water are available in published literature. However, almost all of them are related to the examination of friction and wear behaviour under low contact pressures. Hence, it is imperative to explore the tribological potential of graphene as an additive in water under considerable high contact pressures.

The present study is motivated by a need to unravel the friction and wear behaviour of graphene both as a solid lubricating coating and as an additive water, which is an environmental friendly lubricant. The growth parameters like growth temperature, precursor gas flow rate and reaction time, for chemical vapour deposition of graphene coatings on nickel-catalysed bearing steel, may be varied to understand their effect on the quality of graphene and to attain the optimised conditions for its growth. Similarly, the concentration of graphene oxide in water may be varied by dispersing the different amounts of graphene oxide in water, in order to understand the effect of varying concentration on the rheological as well as tribological behaviour of the lubricant. In order

to determine the friction and wear behaviour of synthesised graphene, bearing steel has been selected as the substrate as well as the counterface. On the other hand, a tribo-pair of the stainless steel discs-stainless steel ball has been selected to investigate the friction and wear behaviour of graphene oxide-water dispersion.

In the light of above, the present study has been conducted with the aim to fulfil the objectives.

i. To synthesise and characterise the graphene films by thermal chemical vapour deposition on bearing steel catalysed with a layer of electroplated nickel and to optimise the temperature, gas flow rate, and reaction time.
ii. To explore the tribological behaviour of the optimised grown graphene films under rotary conditions for short as well as long duration.
iii. To evaluate the friction and wear performance by conducting tests under dry reciprocating sliding for optimised grown graphene under different loads.
iv. To explore the tribological potential of graphene oxide nano-sheets as an additive in water under reciprocating sliding.
v. To establish the dominating mechanisms of wear.